

Bio-Inspired Icephobic Coatings for Aircraft Icing Mitigation: A Critical Review

Liqun Ma, Zichen Zhang, Linyue Gao, Yang Liu and Hui Hu*

Department of Aerospace Engineering, Iowa State University, Ames, IA 50011-2271, USA

Abstract A critical review is provided to summarize our recent efforts to utilize the state-of-the-art bio-inspired icephobic coatings/surfaces, i.e., 1). Lotus-leaf-inspired superhydrophobic surfaces (SHS) and 2). Pitcher-plant-inspired slippery liquid-infused porous surfaces (SLIPS) for aircraft icing mitigation. By leveraging the unique Icing Research Tunnel of Iowa State University (i.e., ISU-IRT), an experimental campaign was performed to evaluate the effectiveness of using SHS and SLIPS coatings to suppress impact ice accretion over the surfaces of typical airfoil/wing models. While both SHS and SLIPS were found to be able to suppress ice accretion over the airframe surfaces where strong aerodynamic forces are exerted, ice was still found to accrete in the vicinity of the airfoil stagnation line where the aerodynamic forces are at their minimum. A novel hybrid anti-/de-icing strategy concept to combine icephobic coatings with minimized surface heating near airfoil leading edge was demonstrated to effectively remove impact ice accretion over entire airfoil/wing surfaces. An experimental investigation was also conducted to examine the durability of the icephobic coatings/surfaces to resist “rain erosion” effects (i.e., the damage to the surface coatings due to continuous impingement of water droplets at high speeds) in considering the practical usage for aircraft icing mitigation. The rain erosion effects were characterized based on the variations of the ice adhesion strengths and surface morphology of the eroded test surfaces coated with SHS and SLIPS. The research findings are very helpful to elucidate the underlying physics for the development of novel and robust anti-/de-icing strategies for aircraft icing mitigation.

Keywords Aircraft icing phenomena, impact icing process, bio-inspired icephobic coatings/surfaces, rain erosion effects, durability of icephobic coatings/surfaces

*Corresponding author: huhui@iastate.edu

7.1 Introduction

Aircraft icing has been widely recognized as a severe weather hazard to flight safety in cold climate. The most frequently observed aircraft icing events are the ice-buildup over airframe surfaces when airplanes are exposed to frozen precipitation at airports, which can be overcome by applying anti-/de-icing fluids over the airframe surfaces prior to takeoff [1]. Aircraft inflight icing occurs when small, super-cooled, airborne water droplets, which make up clouds and fog, freeze upon impacting onto airframe surfaces, as shown schematically in Figure 7.1. Ice accumulation over airframe surface was found to degrade the aerodynamic performance of an airplane significantly by increasing drag while decreasing lift [2]. In moderate to severe conditions, an airplane can become so iced up that continued flight is impossible [3]. The airplane may stall at much higher speeds and lower angles of attack than normal. It can roll or pitch uncontrollably, and recovery may be impossible. The importance of proper ice control for aircraft operation in cold climate was highlighted by many aircraft crashes in recent years like the Continental Connection Flight 3407 crashed in Buffalo, New York on February 14, 2009 due to ice buildup on its wings killing all 49 people aboard and 1 person on the ground as the plane hit a residential home [4]. While noticeable research progress has been made in recent years in providing better understanding about aircraft icing phenomena, aircraft icing remains as an important unsolved problem at the top of the National Transportation Safety Board's most wanted list of aviation safety improvements.

While the airborne water droplets in the clouds are in a super-cooled state, they can either freeze immediately or become mixtures of liquid water and ice upon impinging onto airframe surfaces, depending on the ambient conditions [5]. As clearly shown in Figure 7.1(a), with the cloud having a low liquid water content (LWC) and micro-sized super-cooled water droplets being at relatively low ambient temperatures (i.e., typically below $-10\text{ }^{\circ}\text{C}$), rime ice would usually form over the airframe surface, as the super-cooled water droplets would freeze immediately upon impact. Due to the immediate freezing of the impacted water droplets, air bubbles may be trapped among the ice grains, resulting in the appearance of the rime ice to be opaque, and milky white in color [6]. Under rime icing conditions, the released latent heat of fusion during the solidification process of the impacted

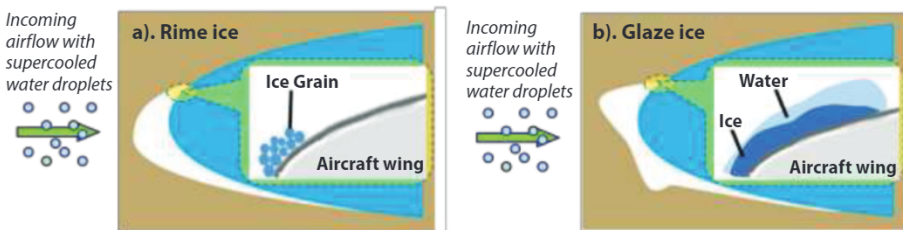


Figure 7.1 Rime ice and glaze ice over an airframe surface.

super-cooled water droplets would be removed rapidly through heat transfer process, and no obvious traces of runback water flow would exist over the airframe surfaces. The total amount and ice accretion rate over the airframe surfaces would be solely determined by the impinging behavior of the super-cooled water droplets [5]. Glaze icing usually occurs when aircraft encounters clouds with relatively warmer ambient temperatures (i.e., just below the freezing point of water), higher liquid water contents, and larger super-cooled water droplets. Under glaze icing conditions, since the released latent heat of fusion associated with the solidification of the impinged super-cooled water droplets cannot be dissipated fast enough by the heat transfer process, only a portion of the impinged water mass would freeze into ice upon impact, as shown in Figure 7.1(b). The remaining portion of the impinged water mass would remain in liquid form, and run back quickly, driven by the boundary layer airflow over the airframe surface [5, 7, 8]. As a result, the total amount and ice accretion rate over the airframe surfaces are mainly determined by the capability of the heat transfer process to dissipate/remove the released latent heat of fusion of the impinged super-cooled water droplets over the ice accreting surface [9]. Glaze is the most dangerous type of ice. Because of its wet nature, glaze ice would form much more complicated shapes which are very difficult to accurately predict, and the resulting ice shapes tend to substantially deform the ice accreting airframe surface with the formation of “horns” and larger “feathers” growing outward into the airflow [7, 10, 11]. As a result, glaze ice formation will severely decrease the airframe aerodynamic performance by causing large scale flow separations, causing dramatic lift reduction and drag increase [2].

Various anti-/de-icing systems have been developed in recent years to ensure safe and efficient aircraft operation in atmospheric icing conditions. While anti-icing refers to the prevention of any buildup of ice on an airframe surface, de-icing denotes the cases where ice has already formed on an airframe surface, which is subsequently removed. All aircraft anti-/de-icing systems can generally be classified into two categories: active and passive methods. While active methods rely on energy input from an external system for the anti-/de-icing operation, passive methods take advantage of the physical properties of the airframe surfaces (e.g., surface wettability) to prevent/delay ice formation and accretion. Current active anti-/de-icing strategies for aircraft icing mitigation suffer from various drawbacks. For example, aqueous solutions of propylene and ethylene glycol (minimum 50% concentration) along with other chemical additives are widely used for aircraft anti-/de-icing at airports. Propylene and ethylene glycol, although readily biodegradable, exert an extremely high biochemical oxygen demand on aquatic systems that results in killing fish and other aquatic creatures due to the depletion of dissolved oxygen [12]. There has been an increasing concern for the environmental impacts from the aircraft anti-/de-icing fluid swept away with storm and melt-water runoff at airports to ground water and nearby waterways [13]. Pneumatic de-icing systems with rubber boots have been used to break off ice chunks accreted at airframe leading edge for aircraft in-flight icing mitigation, but they are usually

quite heavy and sometimes unreliable [1]. Ultrasonic and mechanical de-icing solutions are not easily integrated into existing aircraft and pose foreign object damage (FOD) hazards to engines [1]. While electric-thermal or hot air bleeding systems have been used to melt out ice by heating massive wing surfaces, they are usually very inefficient and have demanding power requirements and can also cause damage to composite airframes from overheating. Furthermore, the water from the melt ice may simply run back and re-freeze at further downstream locations to cause uncontrolled ice accretion [1]. Thus, it is highly desirable to develop more effective and robust anti-/de-icing strategies with minimized power requirements and adverse environmental impacts for aircraft icing mitigation.

Passive anti-icing approaches using icephobic surface coatings are currently being investigated for use as viable strategies for aircraft icing mitigation. Based on the surface structures and anti-icing mechanisms, most of the state-of-the-art icephobic coatings/surfaces can be generally divided into two categories: 1). Lotus-leaf-inspired superhydrophobic surfaces (SHS) with micro-/nano-scale surface textures; 2). Pitcher-plant-inspired slippery liquid-infused porous surfaces (SLIPS) with a layer of liquid lubricant (which is immiscible with water) sandwiched between ice and solid substrate material. While the icephobic coatings/surfaces have been demonstrated to be icephobic under rather static icing conditions for anti-frosting applications, their capability for impact icing mitigation (i.e., ice formed due to the dynamic collision of supercooled water droplets onto a solid surface at high impacting speeds) pertinent to aircraft inflight icing phenomena has not been fully explored. Furthermore, the durability of the icephobic coatings/surfaces to resist rain erosion effects (i.e., the structural damages to the coating materials due to the continuous impingement of water droplets) has not well investigated either.

In the present review, we report the progress made in our recent efforts to explore and evaluate the anti-icing performances of the state-of-the-art icephobic coatings/surfaces for aircraft inflight icing mitigation. By leveraging Icing Research Tunnel of Iowa State University (i.e., ISU-IRT), a comprehensive experimental campaign was performed to evaluate the effectiveness of using the icephobic coatings/surfaces to mitigate ice formation/accretion over the surfaces of airframe/wing models. An experimental investigation was also conducted to characterize the durability of the icephobic coatings/surfaces in resisting rain erosion damages caused by the high-speed impingement of water droplets. By using the icephobic coatings/surfaces, a novel hybrid anti-/de-icing strategy concept (i.e., combining icephobic coatings with minimized leading-edge heating) is also explored to effectively prevent ice accretion over airframe surfaces at much lower power costs than the present costly surface heating methods.

7.2 The State-of-the-Art Icephobic Coatings/Surfaces

While various hydro-/ice-phobic coatings/surfaces have been developed in recent years [14–16], almost all the “state-of-the-art” icephobic coatings/surfaces

can be generally divided into two categories, i.e., (a). Lotus-leaf-inspired superhydrophobic surfaces with micro-/nano-scale surface textures to achieve very high contact angles (typically $> 150^\circ$) [17]; and (b). Pitcher-plant-inspired slippery liquid-infused porous surfaces (SLIPS) with a layer of liquid lubricant (which is immiscible with water) being sandwiched between ice and solid substrate materials [18], as shown schematically in Figure 7.2.

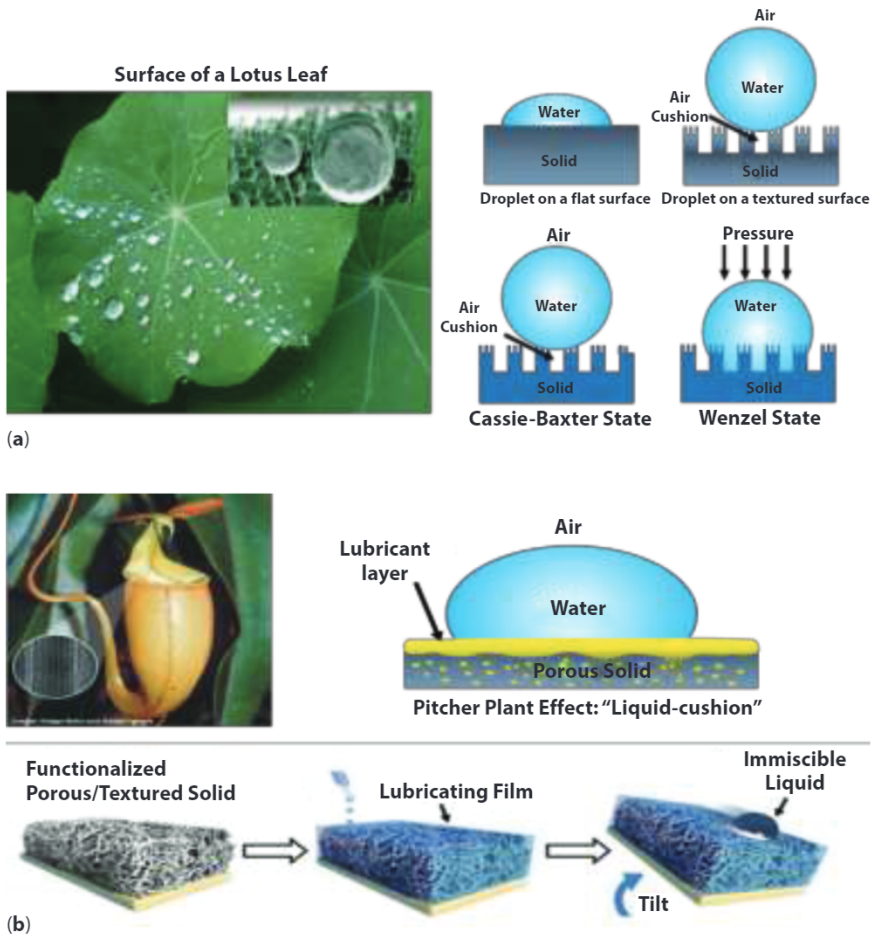


Figure 7.2 Two categories of bio-inspired icephobic coatings/surfaces: (a) Lotus-leaf-inspired superhydrophobic surface (SHS) [19–22], (b) Pitcher-plant-inspired slippery liquid-porous surface (SLIPS) [18, 23, 24].

7.2.1 Lotus-Leaf-Inspired Superhydrophobic Surfaces (SHS) with Micro-/Nano-Scale Surface Textures

Inspired by the outstanding self-cleaning capability of lotus leaf and duck feather, a number of studies have been conducted in recent years to develop coatings to make superhydrophobic surfaces, on which water droplets bead up with a very large contact angle (i.e., $> 150^\circ$) and drip off rapidly when the surface is slightly inclined [19–22, 25]. One attractive application of superhydrophobic surfaces, in addition to the extraordinary water-repellency, is their potential to reduce accumulation of snow and ice on solid surfaces. Under low humidity conditions, some superhydrophobic surfaces were found to show very promising behaviors in delaying ice formation [16, 26] even at temperatures as low as -25 to -30°C [27].

Typically, hydrophobic (i.e., water repellent) materials display lower ice adhesion strength in comparison to hydrophilic (i.e., water loving) materials. Here, ice adhesion strength refers to the shear stress required to separate and remove ice from a surface. This can be explained from a thermodynamic perspective by invoking the work of adhesion. The work of adhesion W_{adh} between ice and a solid material is given as, $W_{adh} = \gamma_{ia} + \gamma_{sa} - \gamma_{si}$, where γ_{ia} is ice surface free energy (i.e., ice-air interfacial free energy), γ_{sa} is the solid surface free energy (i.e., solid-air interfacial energy) and γ_{si} is the solid-ice interfacial free energy. Recognizing that the ice surface free energy ($\gamma_{ia} = 75 \text{ mJ/m}^2$) is approximately equal to the water surface free energy (or surface tension, $\gamma_{wa} = 72 \text{ mJ/m}^2$) and assuming that the surface-ice interfacial free energy γ_{si} is approximately equal to the surface-water interfacial free energy γ_{sw} [28–30], the work of adhesion can be rewritten as $W_{adh} \approx \gamma_{wa} + \gamma_{sa} - \gamma_{sw}$. The hydrophobicity or hydrophilicity of a non-textured solid material is given by the Young's equation [31] as $\gamma_{wa} \cos \theta_Y = \gamma_{sa} - \gamma_{sw}$, where θ_Y is the Young's contact angle of water on the solid surface. By combining the Young's equation with the work of adhesion, $W_{adh} \approx \gamma_{wa} (1 + \cos \theta_Y)$ can be obtained. From this equation, it is evident that non-textured hydrophobic materials with $\theta_Y > 90^\circ$ display lower adhesion to ice in comparison to hydrophilic materials $\theta_Y < 90^\circ$. Thus, it is not surprising that, over the past few decades, many researchers [30, 32–36] have reported lower ice adhesion strength with hydrophobic materials, in comparison to hydrophilic materials. Mittal [37] has discussed the relationship between wettability (surface free energy, work of adhesion) and bond strength in general. Typically, non-polar materials with low solid surface free energy (e.g., hydrocarbons, fluorocarbons) tend to be hydrophobic, and consequently constitute a common choice of materials for the applications requiring low adhesion to ice. However, even the best rigid, non-textured hydrophobic materials display ice adhesion strength on the order of 100 kPa or higher [28].

To develop novel materials/surfaces with lower ice adhesion strength, some researchers naively suggested that superhydrophobic (i.e., extremely water-repellent) materials/surfaces would directly lead to lower ice adhesion. It is well known that all superhydrophobic materials possess textured or rough surfaces

[38–43]. When a macroscopic water droplet comes in contact with a textured superhydrophobic material, it adopts the so-called *Cassie-Baxter state* [43–45] with air trapped in the surface texture beneath the water droplet, as shown in Figure 7.2(a). Since the macroscopic water droplet is supported on thousands of pockets of air, it beads up and displays very high contact angles (typically $> 150^\circ$). However, microscopic water droplets may condense from the surrounding humid air within the surface textures of the superhydrophobic materials to form the so-called *Wenzel state* [46], with water completely wetting the pores or asperities of the textures, as also shown in Figure 7.2(a). Furthermore, super-cooled water droplets impacting onto textured surfaces at high speeds would also readily penetrate the surface textures (i.e., transition from the Cassie-Baxter state to the fully wetted Wenzel state). Under icing conditions, once water freezes within the textures in the Wenzel state, it is extremely difficult to remove the ice, even more than on non-textured surfaces, because of the interlocking between ice and the textures [41, 47–50]. Consequently, some superhydrophobic surfaces were found to display even higher ice adhesion strengths in comparison to non-textured surfaces, substantially increasing the amount of energy required to remove the accreted ice structures [30, 42, 51, 52]. Furthermore, since the airframe surfaces would be exposed to the high-speed impact of supercooled water droplets for a relatively long time, the “rain erosion” resistance performance of SHS coatings (i.e., the ability to prevent the wearing away of the coatings from the substrates by the continuous impact of water droplets) would also be very critical for considering a practical usage of SHS coatings to reduce or eliminate ice accretion over the airframe surfaces. In summary, superhydrophobicity with a textured surface does not necessarily always imply icephobicity, especially for the applications pertinent to aircraft in-flight icing scenario involving high-speed impacts of super-cooled water droplets onto airframe surfaces.

7.2.2 *Pitcher-Plant-Inspired Slippery Liquid-Infused Porous Surfaces (SLIPS)*

Another strategy to reduce ice adhesion strength to a solid surface is to use a layer of liquid lubricant, which is immiscible with water, between ice and the solid surface. The use of such lubricated surfaces was investigated as early as 1960s [53], and has gained increasing attention again recently with the introduction of a concept called Slippery Liquid-Infused Porous Surfaces (SLIPS) [18, 23, 24]. The concept of SLIPS is inspired by the *Nepenthes* pitcher plants, which have evolved highly slippery, liquid-infused micro-textured rim to capture insects [54]. As shown schematically in Figure 7.2(b), a SLIPS consists of a continuous film of lubricating liquid locked in place by a micro/nano-structured substrate, which can repel immiscible liquids that come into contact. The premise of the SLIPS design is that a lubricated surface is intrinsically smooth and defect-free down to the molecular scale, thus provides immediate self-repair by wicking into damaged sites via the

underlying substrate. The liquid-lubricant is largely incompressible, and can be chosen to repel immiscible liquids of virtually any surface tension. Owing to its ultra-smooth surface, SLIPS exhibits many features that outperform conventional coatings [22, 23], which include negligible adhesion to various liquids; rapid and repeatable self-healing; super-repellency at extreme pressure (up to ~ 676 atm); low adhesion to insects, graffiti, and synthetic adhesives [55]. The SLIPS-coated surfaces were not only found to be able to suppress ice/frost accretion by effectively removing condensed moisture even in high humidity conditions, but also exhibit much lower ice adhesion (i.e., ~ 15 kPa at -20°C) than the state-of-the-art superhydrophobic surfaces (SHS). Since the inception of SLIPS, it has inspired a number of coating technologies utilizing infused liquids on or within solids surfaces for enhanced anti-icing performance, which include hygroscopic structured surfaces [50, 56, 57], magnetic slippery surfaces [58] and soft materials/surfaces [59, 60].

It should be noted that one concern about SLIPS for anti-/de-icing applications is the sacrificial nature of the liquid lubricant. The infused liquid could eventually be depleted by evaporation at elevated temperature or at reduced pressure [36]. As ice slides past the lubricated surface, a portion of the liquid lubricant may also be shaved off by the surface of ice (i.e., cohesive failure, as shown schematically in Figure 7.3, demoting the longevity of the lubricated materials [60]. It should also be noted that a novel self-lubricating liquid water layer (SLWL) based anti-icing coating has been developed recently to address this concern, specifically by employing hydrophilic polymers to lock in a thin layer of water on the surface to act as the lubricant [56, 61]. Since the water can be supplied by ice continuously, there will be no concern over the depletion of the lubricant [61]. Another concern is the durability of the SLIPS upon mechanical contact or “rain erosion” effects due to high-speed impacting of water droplets, which can potentially damage the porous substrate and deplete the infused liquid, thus degrading the mechanical integrity of the surface [36].

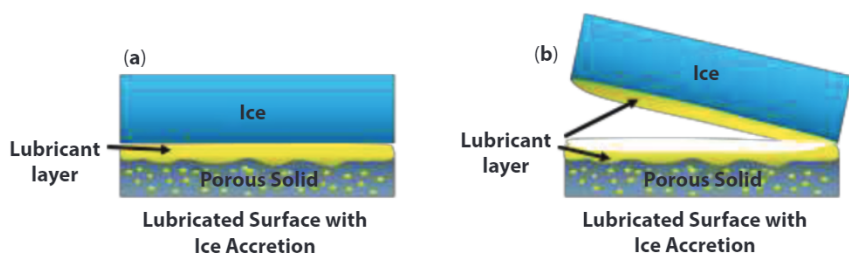


Figure 7.3 Schematics to show the sacrificial nature of SLIPS. (a) lubricant layer being sandwiched between the ice and porous solid substrate; (b) liquid lubricant being shaved off due to the ice shedding.

7.3 Impact Icing Process Pertinent to Aircraft Inflight Icing Phenomena

While both the Lotus-leaf-inspired SHS with micro-/nano-scale surface textures and Pitcher-plant-inspired SLIPS were reported to show very promising performance in delaying ice formation, almost all the previous studies were conducted in a relatively static environment and under very low shearing conditions (i.e., by hand spraying water droplets or pouring water onto substrates and then freezing the test samples in refrigerators) to demonstrate their hydro-/ice-phobic characteristics for anti-frosting applications [62, 63]. Very little work has been done to evaluate the icephobic capability of the coatings/surfaces for “*impact icing*” mitigation pertinent to aircraft inflight icing phenomena, under either dry rime or wet glaze icing condition. Here, the “*impact icing*” is defined as the ice formation process due to the dynamic collision of super-cooled water droplets onto solid surfaces at high impacting speeds. Figure 7.4 gives a comparison of typical ice formed in a rather static environment against the ice structures accreted under different impact icing conditions. As shown clearly in Figure 7.4(a), for the ice sample formed under a relatively stable cooling/freezing environment with controllable water deposition condition, it appears to be clear and transparent. The ice adhesion strength to the substrate is also quite uniform along the interface. In comparison, as revealed clearly in Figure 7.4(b), the ice structures formed under dynamic impact icing conditions were found to vary significantly, depending on the conditions in which the ice was formed. Air temperature, air speed, water droplet size, liquid water content in the airflow, and airframe geometry all would affect the ice structures that accrete.

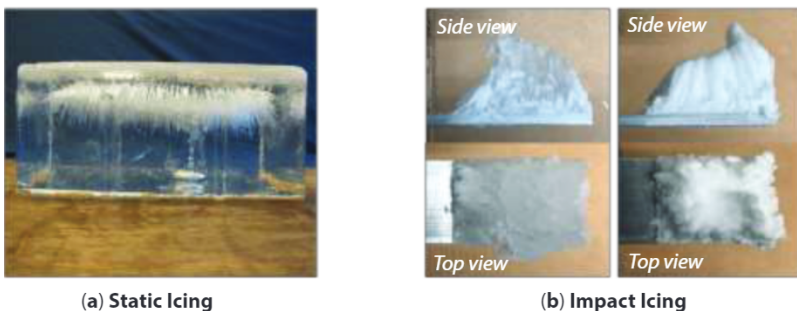


Figure 7.4 (a) Ice sample formed under a static icing condition which has a relatively stable cooling/freezing environment and controllable water deposition process; (b) Ice structures accreted over a rotating blade surface due to dynamic impacting of droplets onto the rotating blade surface under different test conditions (i.e., left: at the temperature of $-5\text{ }^{\circ}\text{C}$ and rotational speed of 3,000 rpm; right: at the temperature of $-15\text{ }^{\circ}\text{C}$ and rotational speed of 3,000 rpm) which appear to be significantly different in terms of icing morphology.

Fundamentally, impact icing process is a very complex, multiphase flow phenomenon. The dynamic interactions among multiphase flows (i.e., gas phase - air, liquid phase - water, and solid phase - ice) were coupled with transient phase changing process (i.e., solidification of impacted water) and unsteady heat transfer (i.e., release of the latent heat of fusion), which makes the impact ice accretion process much more complicated, in comparison to the ice formation process under a relatively static condition. Figure 7.5 shows some typical ice structures accreted over the surface of an airfoil/wing model after undergoing 10 minutes of the impact ice accretion experiments with the same incoming airflow speed $V_\infty = 40$ m/s, and ambient temperature $T_\infty = -5$ °C, but having different liquid water content (LWC) levels in the airflow, i.e., (a) $LWC = 0.5$ g/m³, (b) $LWC = 1.0$ g/m³, (c) $LWC = 1.5$ g/m³. It clearly demonstrated that the ice structures accreted over the surface of the same airfoil/wing model would be affected by the icing conditions significantly. While the substantial variations of the impact ice structures revealed in Figure 7.5 resulted from varying the LWC level in the airflow only, the ice structures accreted over airfoil/wing surfaces would vary much more significantly due to the coupled effects of various controlling parameters, including ambient temperature, airflow speed, droplet size, liquid water content in the airflow, and airfoil geometry. As reported in Liu and Hu [6], corresponding to the variations in water collection efficiency and shear stress exerted by the airflow around the airfoil/wing leading edge under different test conditions, both ice morphology and the total amount of ice mass accreted over the airfoil/wing surface were also found to vary greatly.

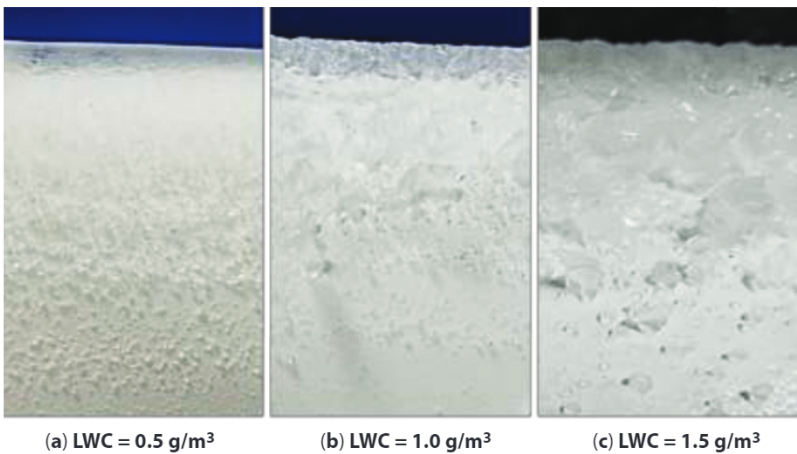


Figure 7.5 Ice structures accreted over an airfoil/wing surface under test conditions with the same airflow velocity $U_\infty = 40$ m/s and temperature $T_\infty = -5$ °C, but different liquid water content (LWC) levels.

7.4 Preparation of Typical SHS and SLIPS Coatings/Surfaces

As aforementioned, almost all the state-of-the-art hydro-/ice-phobic coatings/surfaces can be generally categorized as either a) lotus-leaf-inspired SHS with micro-/nano-scale surface textures [17], or b) pitcher-plant-inspired SLIPS with a layer of water-immiscible liquid lubricant over the surface of the solid substrate [18]. Figure 7.6 gives the schematics of both coatings/surfaces investigated in the present study, i.e., one from each category as the representative cases of the two different kinds of icephobic coatings/surfaces.

As shown schematically in Figure 7.6 (a), a SHS coated test plate was prepared by spraying a commercially available SHS coating - Hydrobead® onto an aluminum test plate. The surface of the test plate was polished with sandpapers according to the ASTM standard (E3-11). The pretreatment could strengthen the bond between SHS and the substrate as well as enhance the homogeneity of the SHS coating. By following the similar procedure as that described in Liu *et al.* [64], both Hydrobead® standard and Hydrobead® enhancer were applied to the surface of the test plate according to the product instruction. As revealed from the Scanning Electron Microscope (SEM) image for the newly treated test surface given in Figure 7.6(a), arrays of micro-/nano-scale surface textures were found to be generated right after spraying the Hydrobead® coating onto the test plate surface. The contact angle of a sessile water droplet on the SHS coated test surface was found to be about 156 degrees (i.e., $\theta \approx 156^\circ$), confirming that the SHS coated test surface is indeed superhydrophobic, as expected.

Figure 7.6(b) gives the schematic of the SLIPS used in the present study. Following the work of Wong *et al.* [23] to make SLIPS, the top surface of the test plate was covered with a thin porous layer. The porous layer was made of a

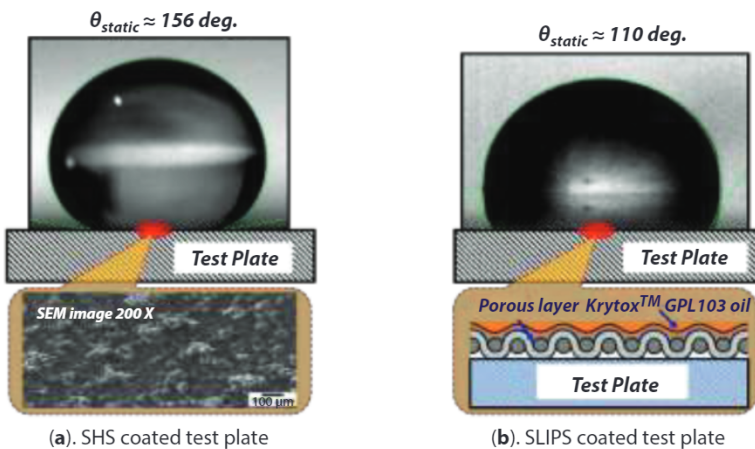


Figure 7.6 Icephobic coatings/surfaces investigated in the present study.

random network of Teflon nanofibrous membrane purchased from Sterlitech®, Seattle, Washington. The hydrophobic membrane was laminated with its functioning surface having an average pore size of less than 200 nm, and it can stick firmly to the surface of the test plate. The lubricating fluid used for the present study was Krytox® 103, which is a clear, colorless perfluorinated oil from DuPont. The slippery oil infused surface had a thickness of 60-80 μm . It should be noted that the Krytox® 103 was also used by Wong *et al.* [23] and Liu *et al.* [65] to make SLIPS due to its low evaporation rate to eliminate the influence of oil depletion from evaporation. Wong *et al.* [23] conducted an experimental study to quantify the evaporation rate of the perfluorinated oil by measuring the liquid mass loss with a high resolution balance. They found that for Krytox® 103, the evaporation rate was less than 0.05% per day and the change in the surface wetting property was negligible over a 28-day period. Therefore, the changes in the surface wettability and durability due to the evaporation of the perfluorinated oil of Krytox® 103 are negligible for the test cases of the present study. It was also revealed clearly that the contact angle of a sessile water droplet on the newly treated surface of SLIPS was found to be about 110 degrees (i.e., $\theta \approx 110^\circ$), indicating that the SLIPS coated test surface was hydrophobic, but not superhydrophobic. Similar findings were also reported by Wong *et al.* [23].

7.5 Measurements of Ice Adhesion Strengths on Different Icephobic Coatings/Surfaces

The performance of the icephobic coatings/surfaces under in-flight conditions is challenging to study, since the harsh environment consisting of micrometer-sized supercooled water droplets carried by frozen-cold airflow impacting onto the airframe surfaces at high speeds is very difficult to duplicate/simulate in benchtop laboratory experiments. Furthermore, the shear stresses acting on the accreted ice structures will depend on the locations and shapes of the ice structures accreted on the airframe surfaces and the turbulent boundary layer airflow above the airframe surfaces. In the present study, we experimentally examined the ice adhesion strength to different icephobic coatings/surfaces in repeatable benchtop tests. By using a measurement technique similar to the one described in Meuler *et al.* [30], the ice adhesion strengths, τ_{ice} , on various test surfaces before and after “rain erosion” test were characterized with a push-to-shear mechanism. The measurement results will provide points of reference to characterize ice adhesion strengths on airframe surfaces under aircraft in-flight icing conditions.

Figure 7.7 shows the schematics of the experimental setup used in the present study to quantify the ice adhesion strengths on the test plates coated with different icephobic coatings. The test rig consists of an environmental chamber to house a digitally-controlled Peltier cooler (TETech CP061 and TC-48-20) and a linear actuator with integrated motion controller (Newport CONEX-LTA-HS) that drives a 40 N force-torque transducer (JR3-30E12A4) to push an aluminum force probe.

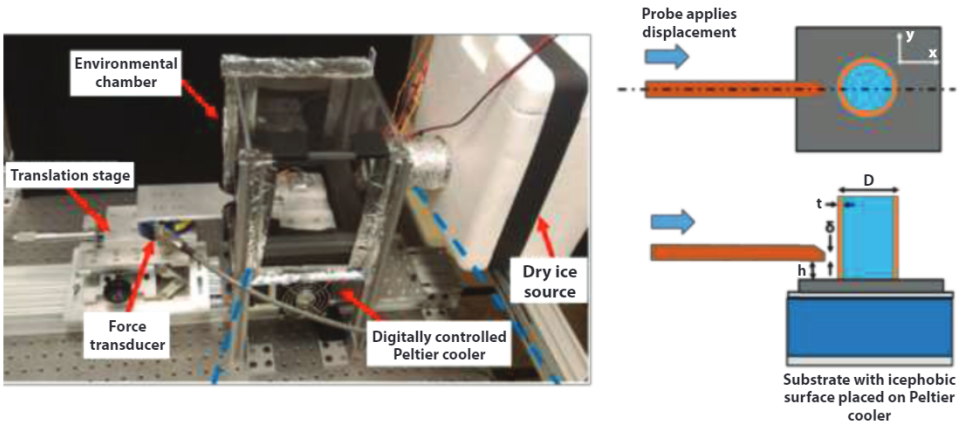


Figure 7.7 Experimental setup to measure the ice adhesion strength on different test surfaces.

The force signals were recorded using a 16-bit data acquisition card (NI PCI-6052E) connected to a host computer. A set of 3D-printed ice molds with 8.0 mm diameter were used to create cylindrical-shaped ice samples on the test plate (i.e., 50 mm \times 50 mm in size). The diagram of a test sample is also illustrated in Figure 7.7, which identifies the diameter of the ice mold cylinder, D , the mold shell thickness, t , the height of the displacement probe, h , and the probe contact height, δ . With the test plate being firmly attached to the Peltier cooler, the surface temperature of the test plate can be well controlled at pre-selected temperatures for the ice adhesion strength measurements (e.g., at $-10\text{ }^{\circ}\text{C}$ for all the test cases in the present study). As also shown schematically in Figure 7.7, the force probe was aligned with the test sample and set at $h = 0.5\text{ mm}$ above the surface of the test plate. A customized MATLAB code was used to record the digital signals given by the force transducer at a data acquisition rate of 2,000 Hz. For each test case, while a tare measurement was performed 10 seconds prior to bringing the force probe into contact with the test sample, the linear actuator stage was set to move at a speed of 0.5 mm/s, until the ice sample was sheared off completely from the surface of the test plate.

Table 7.1 summarizes the measured ice adhesion strengths on various tested surfaces/coatings. Since stainless steel and aluminum are the most commonly used materials to make aircraft parts, the ice adhesion strengths on the polished surfaces of stainless steel and aluminum were also given in the table as the comparison baselines. It should be noted that the measured ice adhesion strength on the polished aluminum surface of the present study was found to be $\sim 450\text{ kPa}$, which is within the range of the measured values reported by Saleem *et al.* [66]. The measured ice adhesion strength for the bare stainless steel surface (i.e., $\tau_{ice} \approx 550\text{ kPa}$) was also found to agree with the measurement results reported by Cao and Hou [9]. The ice adhesion strength on the test surface with enamel coating, i.e.,

Table 7.1 Summary of the measured ice adhesion strengths on various surfaces/coatings.

Test surface	Number of trials	Average ice adhesion strength [kPa]	Standard deviation of ice adhesion strength [kPa]
Aluminium	10	450	±60
Stainless steel	10	550	±130
Enamel	10	1400	±130
SHS-Hydrobead™	10	105	±20
SLIPS	10	35	±10

a very commonly used protective or decorative coating on metal, glass, or ceramic ware, was also measured and found to be $\tau_{ice} \approx 1,400$ kPa. Based on the measurement results given in Table 7.1, it can be seen clearly that the ice adhesion strength on the test surface coated with SHS coating-Hydrobead™ was found to be only $\tau_{ice} \approx 105$ kPa, indicating that the SHS coating is effective in reducing ice adhesion strength on the test surface, in comparison to the uncoated bare metal surfaces (i.e., both stainless steel and aluminum) and conventional enamel coating. The ice adhesion strength on the SLIPS coated surface (i.e., $\tau_{ice} \approx 35$ kPa) was found to be the lowest among all the tested surfaces, as expected.

7.6 Icing Tunnel Testing to Evaluate the Icephobic Coatings/Surfaces for Impact Icing Mitigation

A comprehensive experimental campaign was performed to evaluate the effectiveness of the icephobic coatings (i.e., both SHS and SLIPS) for impact icing mitigation using the Icing Research Tunnel available at Aerospace Engineering Department of Iowa State University (i.e., ISU-IRT). As shown schematically in Figure 7.8, ISU-IRT is a research-grade, multi-functional icing wind tunnel with a test section of 2.0 m in length \times 0.4 m in width \times 0.4 m in height and four transparent sidewalls. It has the capacity of generating airflow at wind speeds up to 60 m/s in the test section and airflow temperatures down to -25 °C. An array of eight pneumatic atomizer/spray nozzles are installed at the entrance of the contraction section of the icing research tunnel to inject micro-sized water droplets (10 ~ 100 μ m in size) into the airflow. By manipulating the pressure and flow rate supplied to the atomizer/spray nozzles, the liquid water content (LWC) in ISU-IRT is adjustable (i.e., LWC ranging from 0.1 g/m³ to 5.0 g/m³). In summary, ISU-IRT can be used to simulate various atmospheric icing phenomena over a range of icing conditions (i.e., from dry *rime* to extremely wet *glaze* ice conditions). Further information about ISU-IRT is available in the studies of Gao *et al.* [67] and Liu *et al.* [68].

By leveraging the unique capability of ISU-IRT, a series of experiments were conducted to evaluate the effects of the icephobic surface coatings on the dynamic ice

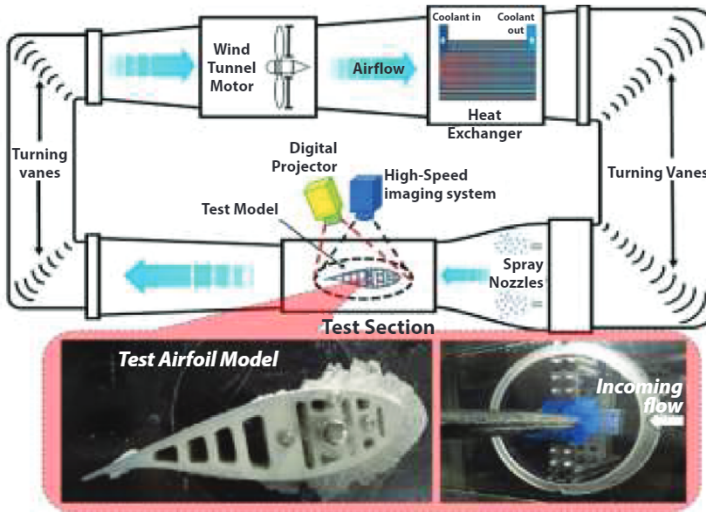


Figure 7.8 Schematic of ISU-IRT used for the present study.

accretion process over the surfaces of airfoil/wing models under different icing conditions pertinent to aircraft inflight icing phenomena. Figure 7.9 shows typical experimental results to reveal the effects of the icephobic coatings (i.e., SHS and SLIPS coatings) on the dynamic ice accretion process over the surface of a typical airfoil/wing model. The experimental study was performed under the impact icing conditions of $V_\infty = 40$ m/s; $T_\infty = -5^\circ\text{C}$; and $LWC = 1.2$ g/m³. The snapshot images were acquired by using the high-speed imaging system to reveal the dynamic ice accreting process over the upper surface of an airfoil/wing model as a function of the ice accretion time. It can be seen clearly that for the test model before applying any icephobic coatings (i.e., the baseline case), upon impacting of the super-cooled water droplets carried by the frozen cold incoming airflow, ice structures were found to accrete very rapidly on the surface of the test model. Under the icing conditions of $V_\infty = 40$ m/s, $T_\infty = -5^\circ\text{C}$, and $LWC = 1.2$ g/m³, the impact icing process was found to be a typical glaze ice accretion process with obvious surface water runback and formation of transparent, glassy ice structures over the airfoil surface, as described in Liu and Hu [6].

It can be clearly seen that in comparison to the baseline case given in Figure 7.9(a), substantially less ice structures were found to accrete over the surface of the airfoil/wing model after coated with the icephobic coatings/surfaces, i.e., for the SHS coated airfoil surface given in Figure 7.9(b), and SLIPS coated airfoil surface given in Figure 7.9(c). The much less ice accretion over the airfoil surfaces after treated with the icephobic coatings is believed to be closely related to the much weaker ice adhesion strength on the icephobic coatings, as listed in Table 7.1. As

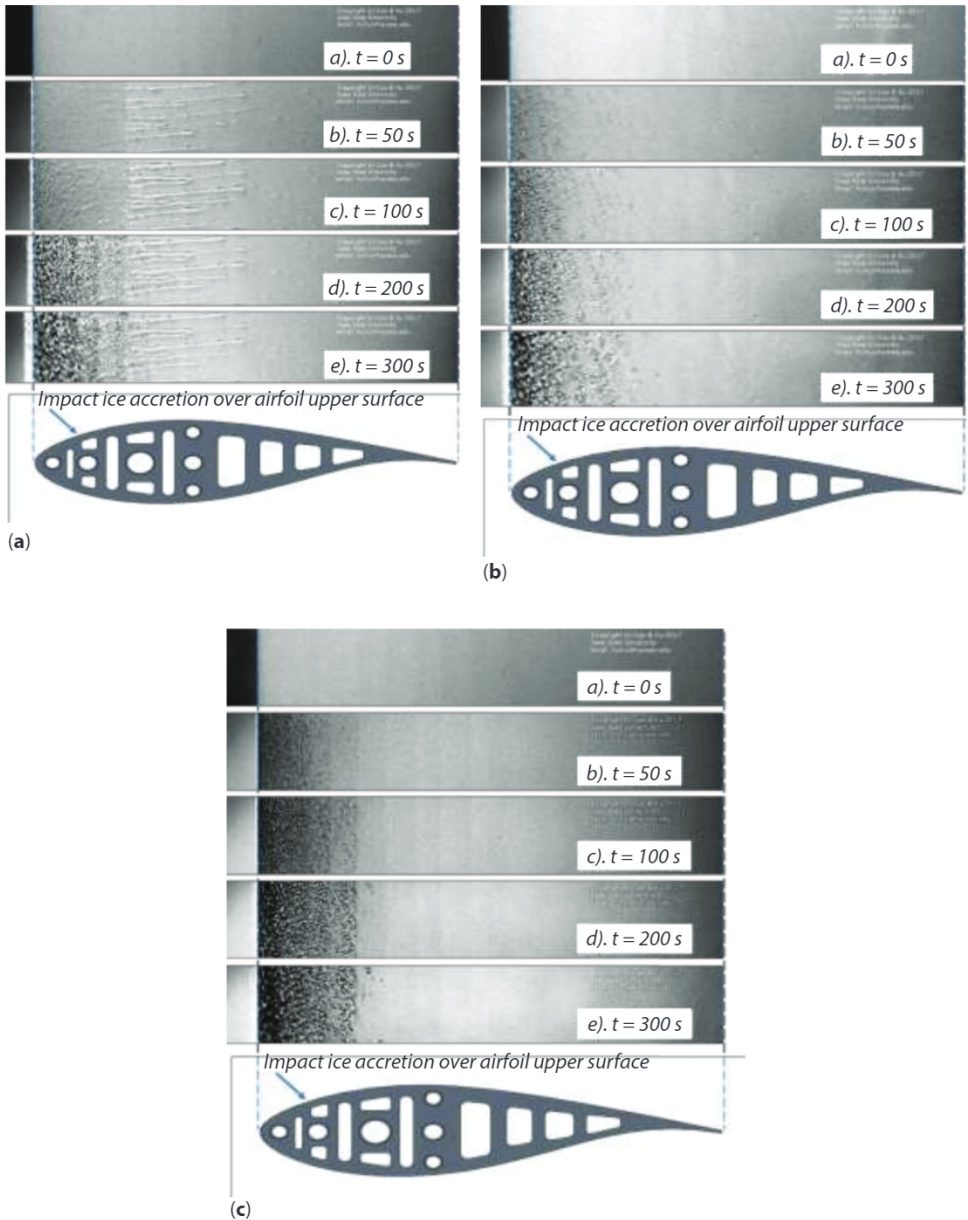


Figure 7.9 Dynamic ice accretion processes over the surface of an airfoil/wing model before and after coated with icephobic SHS and SLIPS coatings. (a) Uncoated airfoil surface as the comparison baseline, (b) Airfoil/wing model coated with SHS, and (c) Airfoil/wing model coated with SLIPS.

a result, the aerodynamic shear stresses from the boundary layer airflow over the airfoil surface would much more readily sweep away the impacted ice mass and ice structures from the airfoil surfaces coated with icephobic coatings, in comparison to the uncoated airfoil surface (i.e., the baseline case). While both SHS and SLIPS coatings were found to be effective in reducing the coverage area by the accreted ice structures over the surface of the airfoil/wing model, the extent of their effectiveness in mitigating impact ice accretion was found to vary noticeably, corresponding to the different surface wettabilities and ice adhesion strengths of the icephobic coatings/surfaces.

It should also be noted that even though the total amount of ice structures accreted over the airfoil/wing surface was found to be much less after applying the icephobic coatings (i.e., either SHS coating or SLIPS) to the airfoil surface, ice structures were still found to form in the region near the leading edge of the airfoil/wing model (i.e., in the vicinity of the airfoil stagnation line). This highlights one of the major challenges faced by the icephobic coating strategies for impact icing mitigation. The icephobic coatings produce low adhesion forces between the impacted water and/or accreted ice and airfoil surface and rely on aerodynamic stresses acting tangentially to the airfoil surface to remove the water/ice accretion. Such approaches would break down at the airfoil stagnation line because the shear stresses near the airfoil stagnation line would be very small or vanish completely. Further exacerbating the problem is that the water collection efficiency is at a maximum at the stagnation line. Once ice starts to accrete along the stagnation line of the airfoil/wing model, the super-cooled water droplets carried by the incoming airflow would directly impact onto the surface of the accreted ice structures, instead of the coated airfoil surface. Therefore, more and more ice structures were found to accrete over the airfoil surface in the region near the airfoil leading edge as the ice accretion time increased. To remove ice accretion from the region near the airfoil stagnation line, the adhesion of ice to the surface must be very low. Currently, this is usually accomplished by airfoil surface heating with electric-thermal heaters or hot air bleeding systems to melt the ice accreted near the airfoil leading edge, thereby reducing/removing the accreted ice from the airfoil surface in the vicinity of the stagnation line.

A hybrid anti-/de-icing strategy that combines icephobic coatings with surface heating only in the minimized region near the airfoil leading edge (LE) is developed recently in order to prevent/remove ice accretion over entire airfoil/wing surface with a minimized power consumption. To demonstrate the outstanding anti-/de-icing performance of the hybrid strategy, a comparative study was conducted to compare the performances of different anti-/de-icing strategies, i.e., a) the baseline case with neither surface heating nor icephobic coating, b) applying icephobic coating but no surface heating; c) applying surface heating near airfoil leading edge but no icephobic coating; d) hybrid strategy to combine icephobic coating with a minimized surface heating near airfoil leading edge. Figure 7.10 shows a side-by-side comparison of the icing tunnel test results after 10 minutes

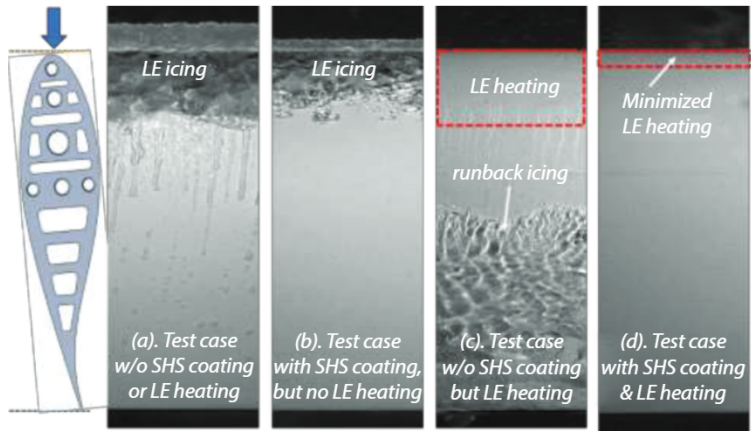


Figure 7.10 Comparison of different anti-/de-icing strategies for impact icing mitigation. LE stands for airfoil leading edge.

of the ice accretion experiments under the impact icing conditions of $V_\infty = 40 \text{ m/s}$; $T_\infty = -5^\circ\text{C}$; and $LWC = 1.2 \text{ g/m}^3$, which clearly reveals the significant differences between the baseline case and those with different anti-/de-icing strategies in terms of the ice accretion over the surface of the same airfoil/wing model. It can be clearly seen that for the baseline case (i.e., without surface heating and uncoated airfoil surface), while large amounts of ice structures were found to accrete in the region near the airfoil leading edge, obvious runback water was also observed over the airfoil surface and froze into rivulet-shaped runback ice structures at further downstream locations, as shown clearly in Figure 7.10(a). It was revealed clearly in Figure 7.10(b) that after applying the icephobic SHS coating to cover the airfoil/wing surface, the aerodynamic stresses from the boundary layer airflow above the airfoil surface were found to sweep away impinged water droplets/accreted ice structures from most of the airfoil surface except in the vicinity of the stagnation line, due to the high impinging pressure and extremely small aerodynamic shear stresses at those locations. Figure 7.10(c) shows clearly that after turning on the heating element flush mounted around the airfoil leading edge, the ice structures accreted in the region near the airfoil leading edge can be eliminated effectively. However, the meltwater was found to simply run back and re-freeze into ice, i.e., form runback ice structures, at further downstream locations. By using the hybrid strategy to combine the icephobic coating with a minimized surface heating near the airfoil leading edge as shown in Figure 7.10(d), it was found that even with a much smaller amount of power input, i.e., only $\sim 20\%$ of the LE heating case given in Figure 7.10(c), the entire surface of the airfoil/wing model was found to be completely free of ice (i.e., no ice accretion in both regions near the airfoil leading edge and the downstream locations over the airfoil surface) during the whole

duration of the ice accretion experiment. In summary, the hybrid anti-/de-icing strategy to combine the icephobic coating with minimized surface heating near the airfoil leading edge was demonstrated to be very effective to mitigate impact icing process pertinent to aircraft inflight icing phenomena. It can effectively prevent ice accretion over the entire airfoil/wing surface at a much lower power cost than conventional massive surface heating methods.

7.7 Characterization of Rain Erosion Effects on the Icephobic Coatings

As aforementioned, while the icephobic coatings/surfaces have been reported to show very promising performances to suppress ice formation and accretion, the durability of the icephobic coatings/surfaces (i.e., the capability of the icephobic coatings/surfaces to withstand harsh working environments) has not been well investigated. More specifically, since airframe surfaces of aircraft would be exposed to the high-speed impacting of super-cooled water droplets for a relatively long time, the “rain erosion” resistance performances of the icephobic coatings/surfaces (i.e., the ability to prevent the coating materials from wearing away by the continuous impingement of water droplets) would be very critical in considering a practical usage of the icephobic coatings for aircraft inflight icing mitigation. In the present study, a comprehensive experimental investigation was also conducted to evaluate the “rain erosion” resistance performances of the icephobic coatings/surfaces, i.e., the lotus-leaf-inspired SHS and the pitcher-plant-inspired SLIPS, in preventing erosion/corrosion caused by the continuous impingement of water droplets at relatively high speeds up to ~ 100 m/s.

Figure 7.11 shows the experimental setup of the rain erosion test rig used to evaluate the rain erosion effects on the two typical icephobic coatings/surfaces. A high-thrust electric ducted fan (EDF, JP Hobby) is installed at the inlet to drive airflow into a circular-shaped wind tunnel. By manipulating the power level supplied to the electric fan, the speed of the airflow exhausted from the wind tunnel nozzle ($D_{\text{nozzle}} = 38$ mm) can be adjusted from ~ 40 m/s to ~ 100 m/s. While a water spray nozzle (BIMV-11002 nozzle) is integrated in the middle section of the wind tunnel, de-ionized (DI) water is supplied to the spray nozzle to generate micro-sized water droplets and inject them into the airflow. By manipulating the water flow rate supplied to the spray nozzle, the liquid water content (*LWC*) level in the airflow can be varied for different test conditions. By varying the pressure settings of the air and water pipelines connected to the water spray nozzle, the size of the water droplets exhausted from the spray nozzle is also adjustable for different applications. For all the test cases of the present study, in order to simulate the rain erosion effects caused by the micro-sized, airborne water droplets in the cloud impinging onto airframe surfaces pertinent to aircraft inflight icing scenario, the size of the water droplets exhausted from the water spray nozzle was set to range from $10 \mu\text{m}$ to $100 \mu\text{m}$ with a median volumetric diameter (*MVD*) being about $20 \mu\text{m}$. It should also be noted that while the *LWC* level for a typical aircraft inflight icing design

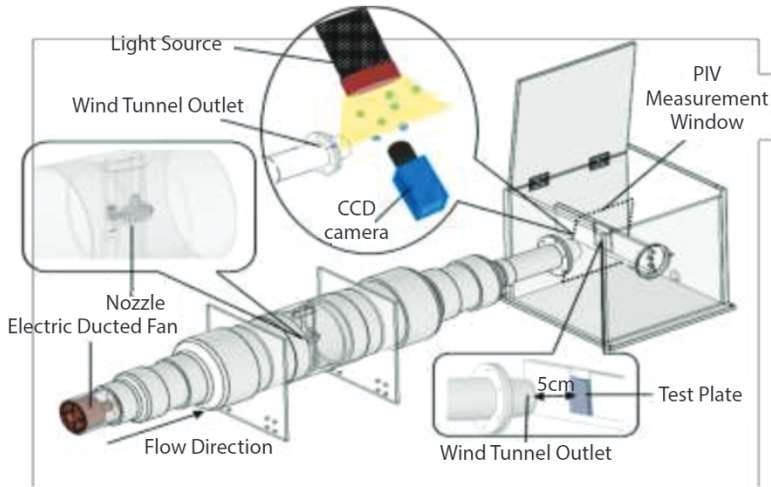


Figure 7.11 Schematic of the test rig to evaluate rain erosion effects on icephobic coatings.

envelope would be about $LWC \approx 0.5 \sim 1.0 \text{ g/m}^3$, the rain erosion test cases of the present study were designed intentionally with much higher LWC levels (i.e., up to 20 times higher with $LWC \approx 10 \sim 20 \text{ g/m}^3$) in order to accelerate the degradation of the icephobic coatings caused by the rain erosion effects.

A high-resolution digital particle image velocimetry (PIV) system was used to quantify the characteristics of the water spray flow exhausted from the wind tunnel nozzle, and some typical PIV measurements are given in Figure 7.12. It can be seen clearly that the flying velocity of the water droplets was found to be rather uniform within the water spray flow, which is almost the same as the freestream airflow velocity (i.e., V_∞). Therefore, the freestream airflow velocity can be referred as the nominal impacting velocity of the water droplets in the present study. It can also be seen that due to the existence of a strong adverse pressure gradient near the impingement point, the droplets were found to decelerate as they approached the test plate, as expected. With continuous impingement of the water droplets onto the test plate, the characteristics of the “rain erosion” effects on the icephobic coatings could be examined quantitatively.

Figure 7.13 gives some snapshot images to reveal the dynamic rain erosion process on the SHS and SLIPS coated test surfaces under the test conditions of $V_\infty = 65 \text{ m/s}$ and $LWC = 15 \text{ g/m}^3$. As shown clearly in Figure 7.13(a), upon impacting of water droplets onto the SHS coated test surface, a bright region (i.e., highlighted by the yellow dash line) was observed in the center of the impacting water spray flow. This is because the hierarchical surface textures over the SHS coated test surface would generate less light reflection before water droplets impacting onto the test surface. However, upon high-speed impingement of the water droplets at

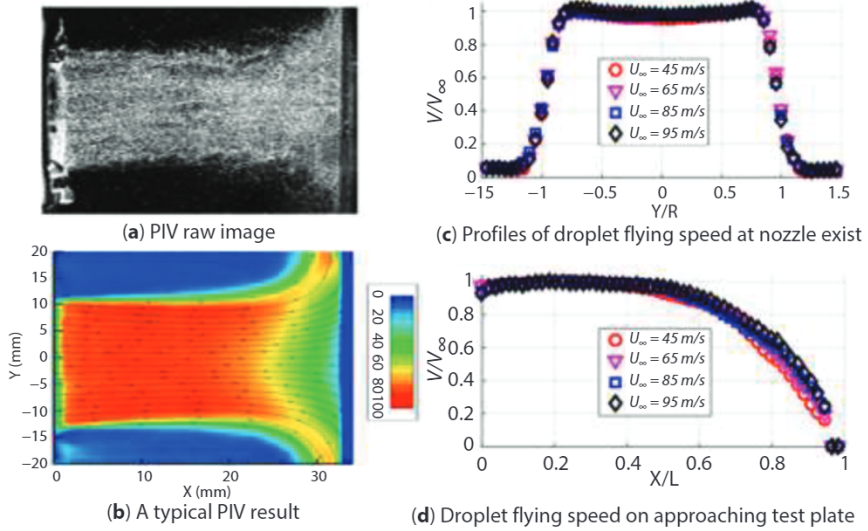


Figure 7.12 PIV measurement results of the impinging water spray flow.

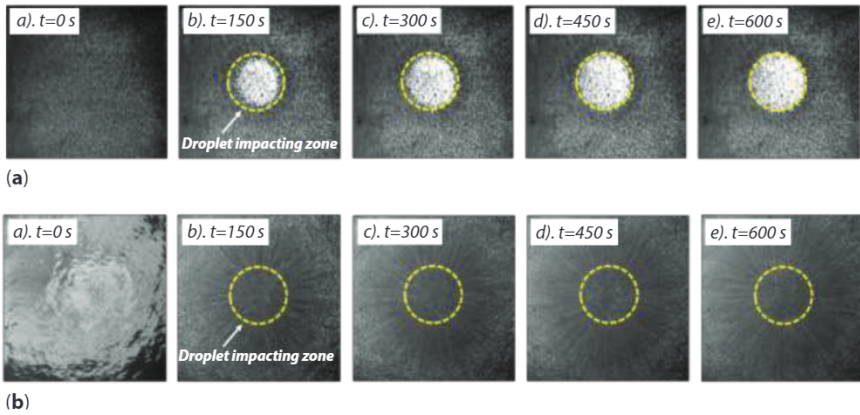


Figure 7.13 Snapshot images to reveal the dynamic rain erosion process on the SHS and SLIPS coated test surfaces with $V_\infty = 65 \text{ m/s}$ and $LWC = 15 \text{ g/m}^3$. (a) Time evolution of the rain erosion process on the SHS coated test surface, (b) Time evolution of the rain erosion process on the SLIPS coated test surface.

$V_\infty = 65 \text{ m/s}$, the hierarchical surface textures would be saturated by the impacted water mass (i.e., transition from the Cassie-Baxter state to the fully wetted Wenzel state), and a water film would be generated in the core region of the impinging water spray flow (i.e., droplet impacting zone). Since more light would be reflected

from the water film over the test surface (i.e., mirror-like nature of the water film), a very bright spot was observed over the SHS coated surface, as shown clearly in Figure 7.13(a). Once the water spray flow was terminated, the water film will be evaporated rapidly by the incoming airflow, and the hydrophobicity of the SHS coated surface could be regained.

The snapshot images given in Figure 7.13(b) show the time evolution of the rain erosion process on the SLIPS coated test surface. Since an excess oil was applied in preparing the SLIPS coated test surface as suggested by Wong *et al.* [23], a very strong reflection of the illumination light was observed from the smooth oil film on the top of the SLIPS coated test plate. As seen clearly from the the snapshot images acquired after starting the rain erosion testing, the excess lubricant oil on the top of the SLIPS coated test plate was found to be flushed away by the impinging water spray flow. It was also revealed clearly that the impinging water droplets would slide away from the stagnation point (i.e., the center of the impinging water spray flow) radially, unless they were trapped inside the porous substrate.

Figure 7.14 gives the measured ice adhesion strengths on the test plates coated with SHS and SLIPS as a function of the duration of the rain erosion testing under the test conditions of $V_\infty = 75 \text{ m/s}$ and $LWC = 13 \text{ g/m}^3$. It can be seen clearly that the ice adhesion strength on the SHS coated test plate was found to increase very rapidly at the earlier stage of the rain erosion testing (i.e., within the first 10 minutes), and then growing gradually with only a moderate rate with increasing duration of the rain erosion testing. More specifically, while the ice adhesion strength on the SHS coated test surface was found to be $\tau_{ice} \approx 105 \text{ kPa}$ before starting the rain erosion testing, the corresponding value was found to increase to $\tau_{ice} \approx 350 \text{ kPa}$ (i.e., ~ 3.5 times greater) after 10 minutes of the rain erosion testing. After 40 minutes of the rain erosion testing, the ice adhesion strength on the SHS coated test surface was found to become $\tau_{ice} \approx 400 \text{ kPa}$, which is still slightly lower than the value

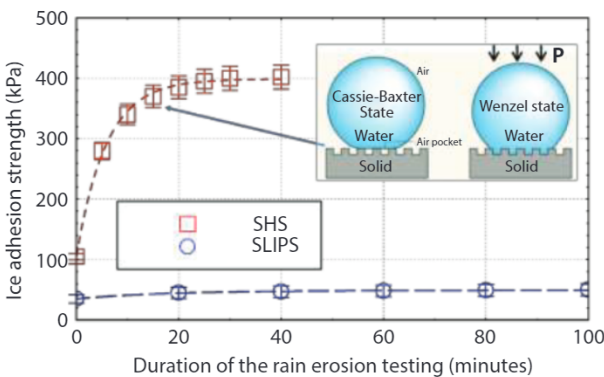


Figure 7.14 Ice adhesion strength to the icephobic surfaces vs. the rain erosion testing duration.

on bare aluminum surface (i.e., the test surface without the SHS coating). It can also be seen clearly that due to the existence of the excess oil on top of the SLIPS coated test plate, the ice adhesion strength on the newly prepared SLIPS surface was found to be only $\tau_{ice} \approx 35$ kPa, (i.e., before undergoing the rain erosion testing). Since the excess oil on the top of the SLIPS coated test plate would be flushed away rapidly upon dynamic impinging of the water droplets as visualized clearly in Figure 7.13(b), the measured ice adhesion strength on the SLIPS coated test surface was found to increase monotonically as the duration of the rain erosion testing increases. More specifically, after 100 minutes of the rain erosion testing under the test conditions of $V_{\infty} = 75$ m/s and $LWC = 13$ g/m³, the corresponding value was found to increase to $\tau_{ice} \approx 50$ kPa, i.e., over 40% increase due to the rain erosion effects.

In order to elucidate the underlying physics behind the measured ice adhesion strength data presented above, the changes in the surface topography of the SHS coated test plate as a function of the duration of the rain erosion testing were also characterized using an Atomic Force Microscopy (AFM) system. Figure 7.15 shows the AFM scanned images to reveal the surface topography changes of the

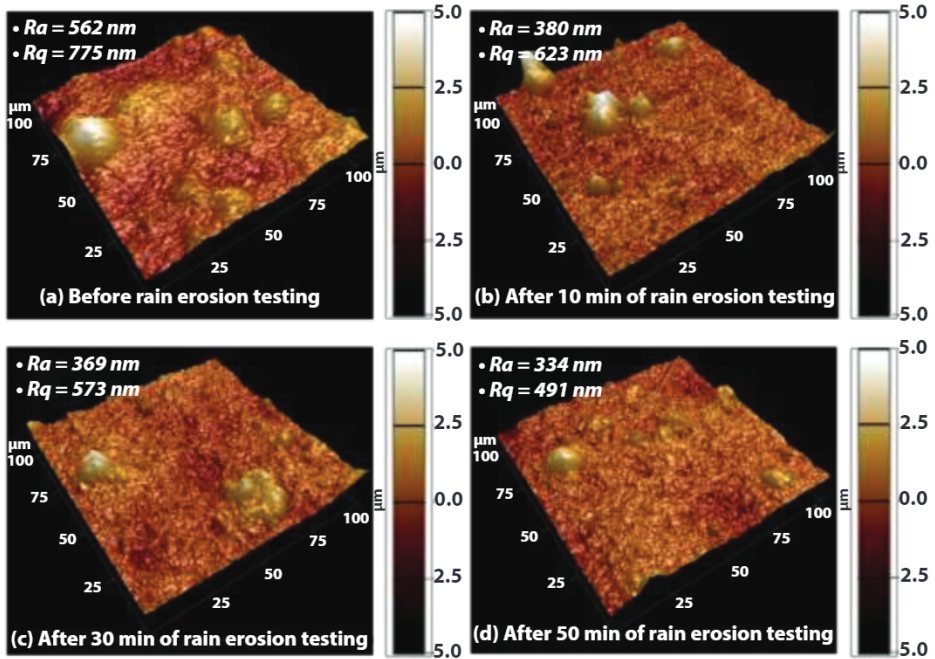


Figure 7.15 AFM images to reveal the surface topography changes of SHS coated test plate caused by the rain erosion effects.

SHS coated test plate before and after undergoing rain erosion testing at different experimental durations (i.e., after 10, 30 and 50 minutes of the rain erosion testing under the test conditions of $V_{\infty} = 65 \text{ m/s}$ and $LWC = 15 \text{ g/m}^3$). Based on the quantitative AFM measurement results as those shown in Figure 7.15, the key parameters to quantify surface topography of the SHS coated test surface, i.e., the averaged surface roughness (R_a) and the corresponding root-mean-square (R_q) values, can be obtained in order to reveal the significant changes in the surface topography of the test plate caused by the rain erosion effects more clearly and quantitatively.

As shown clearly in Figure 7.15(a), nano-/micro-scale textures with different sizes and heights were observed over the SHS coated test plate (i.e., existence of hierarchical textures over the test surface) before the rain erosion testing. It indicates that the SHS coated test surface is rough enough to maintain its superhydrophobicity, as expected. The corresponding surface roughness parameters were found to be $R_a = 562 \text{ nm}$ and $R_q = 775 \text{ nm}$, as given in Figure 7.15(a). However, after undergoing the rain erosion testing, while the texture/roughness structures with relatively smaller size and lower roughness height were still found to be present on the eroded SHS coated test surface, and many large and sharp surface textures (i.e., textures with relatively larger size and greater roughness height) were found to be eroded due to continuous droplet impingement onto the test surface. As a result, the surface roughness parameters on the eroded SHS surface were found to reduce to $R_a \approx 380 \text{ nm}$, 369 nm , and 344 nm , and $R_q \approx 623 \text{ nm}$, 573 nm , and 491 nm , after 10 minutes, 30 minutes and 60 minutes of the rain erosion testing, respectively. It indicates that the eroded SHS coated test surface becomes smoother and smoother, as the duration of the rain erosion testing increases. Corresponding to the vanishing of the hierarchical textures over the eroded test surface, impacting water droplets on the test surface would more readily transition from the partially-wetted *Cassie-Baxter state* to the fully-wetted Wenzel state, eliminating the hydrophobicity of the test surface [69]. Once water freezes within the surface textures in the Wenzel state, it would be very difficult to remove the ice because of the interlocking between ice and the textures [47, 48, 50]. Consequently, as shown quantitatively in Figure 7.14, the ice adhesion strength on the eroded SHS surface was found to increase monotonically with the increasing time of the rain erosion testing.

In order to reveal the underlying physics pertinent to the damage to SLIPS coated test surface induced by the rain erosion effects, two test plates were prepared with their top surfaces covered by two identical porous layers. A comparative study was conducted for water droplets impinging onto both test surfaces under the same test conditions $V_{\infty} = 75 \text{ m/s}$ and $LWC = 13 \text{ g/m}^3$, but with the slippery oil Krytox® 103 being applied to only one of the porous layers. The test case without using the slippery oil to infiltrate into the porous layer (i.e., the dry porous layer case) is used as the baseline for the comparative study. Figure 7.16 gives the snapshot images of the two test surfaces acquired after undergoing the rain erosion testing for the two test cases (i.e., with and without infusing the slippery oil

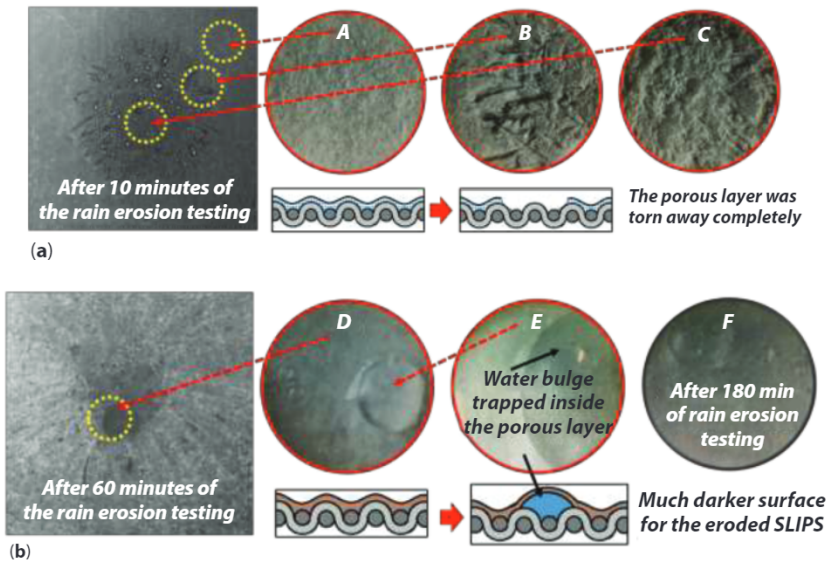


Figure 7.16 Typical rain erosion damages to the SLIPS coated test surface. (a). Without applying the slippery oil to the porous layer, (b). After infusing the slippery oil into the porous layer (i.e., SLIPS surface).

of Krytox® 103 into the porous layers). As shown clearly in Figure 7.16(a), visible structural damages were found to appear much earlier for the “dry” porous layer case (i.e., no lubricant oil was applied to infiltrate into the porous layer). The porous layer was found to be torn up by the impingement of the water droplets within only 10 minutes of rain erosion testing. As indicated by the red dashed circles in the snapshot images, enlarged views in some selected regions are provided in order to reveal the damages to the SLIPS caused by the rain erosion effects more clearly. For the baseline case (i.e., without applying the slippery oil to infiltrate into the porous layer), the undamaged surface of the porous layer in the region far away from the impinging center was found to have relatively smooth surface texture, as revealed clearly in window A. Due to continuous impingement of water droplets, while some fragments of the porous layer were found to be blown away at the edge of the impinging water spray flow, as shown in window B. Corresponding to the much stronger rain erosion effects at the center of the impinging water spray flow, the surface textures of the porous layer were found to be smashed completely and torn away from the substrate surface, as shown clearly in window C.

In comparison to the baseline case, the porous layer on the top surface of the test plate was found to be much more durable after infusing the slippery oil into the porous layer. However, since the infused lubricant oil would be flushed away

gradually due to the continuous impingement of the water droplets, some noticeable damages were found to occur over the SLIPS coated test surface after undergoing about 60 minutes of rain erosion testing. The damages to the SLIPS surface caused by the rain erosion effects were also found to be quite different from those for the dry porous layer case (i.e., the baseline case). As shown clearly in Figure 7.16(b), instead of tearing away the porous layer from the test plate completely, much localized damages were found to be induced by the rain erosion effects to the SLIPS coated test surface. Due to the depletion of the slippery oil from the SLIPS coated surface, the impacted water was found to be able to penetrate into the top porous layer, as revealed from the image given in window D. This could be observed much more clearly from the further enlarged view and schematic given in window E, where both air and water were found to be trapped beneath the top porous layer. As the duration of rain erosion testing became longer and longer, more and more defects were observed on the SLIPS coated test surface. As revealed clearly from the image given in window F, due to the aggregation of damaged fabric elements of the porous layer, the eroded SLIPS was found to become much darker after 180 minutes of rain erosion testing. The wettability of the eroded SLIPS surface was also found to degrade greatly since the damages/contaminants appeared to make the surface of the porous layer hydrophilic. As a result, due to more depletion of the slippery oil and surface damages, the ice adhesion strength to the eroded SLIPS was also found to increase monotonically with increasing time of rain erosion testing, as revealed quantitatively in Figure 7.14.

7.8 Summary and Conclusions

Based on surface structures and anti-icing mechanisms, almost all icephobic coatings/surfaces can be generally divided into two categories: 1). Lotus-leaf-inspired superhydrophobic surface with micro-/nano-scale textures; 2). Pitcher-plant-inspired slippery liquid-infused porous surface (SLIPS) with a layer of liquid lubricant (which is immiscible with water) sandwiched between ice and solid substrate. While various icephobic coatings/surfaces are reported to be very promising in suppressing ice formation under rather static test conditions (i.e., by hand spraying water droplets or pouring water onto substrates and then freezing the test samples in refrigerators) for anti-frosting applications, very little work has been conducted to examine their capabilities to mitigate *impact icing* process (i.e., ice formed due to the dynamic collision of water droplets onto a solid surface at high speeds) pertinent to aircraft inflight icing. In the present review, we summarize the recent research progress made in our recent efforts to explore/evaluate the effectiveness of the state-of-the-art bio-inspired icephobic coatings/surfaces for aircraft inflight icing mitigation.

In the present review, the significant differences between impact icing (which is pertinent to aircraft icing phenomena) and conventional static icing or frosting are highlighted in terms of ice morphology and ice adhesion strength. While

conventional ice samples formed under rather static conditions appear to be clear and transparent with the ice adhesion strength being quite uniform along the ice-substrate interface, morphological appearances of impact ice structures were found to vary significantly depending on the conditions under which the ice structures were formed. Air temperature, airflow speed, water droplet size, liquid water content, and airframe geometry were all found to control the final ice morphology and the resultant ice adhesion strength.

By leveraging the Icing Research Tunnel of Iowa State University (i.e., ISU-IRT), a comprehensive experimental campaign was conducted to evaluate the effectiveness of the icephobic coatings/surfaces in mitigating impact icing process over typical airfoil/wing surfaces pertinent to aircraft inflight icing mitigation. While both SHS and SLIPS coatings were found to be effective to mitigate impact ice accretion over the airfoil/wing surfaces in the regions where strong aerodynamic shear stresses are exerted, substantial ice structures were still found to accrete around the airfoil leading edge (i.e., in the vicinity of the stagnation line) where the aerodynamic shear stresses are at their minimum. The extent of their effectiveness in mitigating impact ice accretion was found to be closely related to the surface wettability and ice adhesion strength of the icephobic coatings/surfaces.

An experimental investigation was also performed to examine the durability of the icephobic coatings/surfaces to resist "rain erosion" effects (i.e., the surface damages due to continuous impingement of water droplets at high speeds) in considering the practical usage of the icephobic coatings for aircraft inflight icing mitigation. It was found that the hierarchical texture structures of SHS coated test surface would be eroded gradually due to the continuous impingement of the water droplets. Corresponding to the vanishing of the hierarchical textures/roughness, water droplets on the eroded SHS surface would more readily transition from the partially wetted *Cassie-Baxter state* to the fully wetted *Wenzel state*. Once water freezes within the surface textures in the *Wenzel state*, it would be very difficult to remove the ice, because of the interlocking between ice and the textures. As a result, the ice adhesion strength to the SHS coated test surface was found to increase exponentially with increasing duration of the rain erosion experiment. For the SLIPS coated test surface, since the slippery oil infused inside the porous layer would be flushed away gradually upon continuous impingement of the water droplets, the impacting water was found to be able to penetrate into the porous layer and accumulate inside porous layer eventually due to the rain erosion effects. Because of the more serious damage/contamination of the SLIPS coated surface induced by the rain erosion effects, the ice adhesion strength on the eroded SLIPS was also found to increase monotonically with increasing time of rain erosion testing.

A novel hybrid anti-/de-icing strategy by combining icephobic coatings with minimized leading edge heating was also explored/demonstrated to effectively remove the ice accretion over the entire airfoil surface at a much lower power consumption than conventional surface heating methods for aircraft icing mitigation.

The findings from the present study are believed to be very helpful to elucidate the underlying physics for the development of novel and robust anti-/de-icing strategies to ensure safer and more efficient operations of aircraft in cold weather.

Acknowledgments

The work summarized here was partially supported by Iowa Energy Center for Wind Turbine Icing Study under the IEC Competitive Grant # 312350, National Aeronautics and Space Administration (NASA) under the grant number NNX16AN21A, and National Science Foundation (NSF) under award numbers CMMI-1824840 and CBET-1916380.

References

- [1] S.K. Thomas, R.P. Cassoni, and C.D. MacArthur, Aircraft anti-icing and de-icing techniques and modeling, *J. Aircraft*. **33**, 841–854(1996).
- [2] M. Bragg, G. Gregorek, and J. Lee, Airfoil aerodynamics in icing conditions, *J. Aircraft*. **23**, 76–81(1986).
- [3] M.G. Potapczuk, Aircraft icing research at NASA Glenn Research Center, *J. Aerosp. Eng.* **26**, 260–276(2013).
- [4] F. Mosher, D. Schaum, C. Herbster, and T. Guinn, Analysis of causes of icing conditions which contributed to the crash of Continental Flight 3407, in: *Proc. 14th Conference on Aviation, Range, and Aerospace Meteorology*, Atlanta, Georgia, 2010 (2010).
- [5] R.J. Hansman and M.S. Kirby, Comparison of wet and dry growth in artificial and flight icing conditions, *J. Thermophys. Heat Transfer*. **1**, 215–221(1987).
- [6] Y. Liu and H. Hu, An experimental investigation on the unsteady heat transfer process over an ice accreting airfoil surface, *Int. J. Heat Mass Transfer*. **122**, 707–718(2018)
- [7] G. Fortin, J.-L. Laforte, and A. Ilinca, Heat and mass transfer during ice accretion on aircraft wings with an improved roughness model, *Int. J. Thermal Sci.* **45**, 595–606(2006).
- [8] R. Hansman, and S. Turnock, Investigation of surface water behavior during glaze ice accretion, *J. Aircraft*. **26**, 140-147(1989).
- [9] Y. Cao and S. Hou, Extension to the Myers model for calculation of three-dimensional glaze icing, *J. Aircraft*. **53**, 106–116(2015).
- [10] G. Fortin and J. Perron, Wind turbine icing and de-icing, AIAA-2009-0274, in *Proc. 47th AIAA Aerospace Science Meeting Including New Horizons Forum Aerosp. Expo.*, Orlando, Florida (2009).
- [11] M.K. Politovich, Predicting glaze or rime ice growth on airfoils, *J. Aircraft*. **37**, 117-121(2000).
- [12] D.M. Ramakrishna and T. Viraraghavan, Environmental impact of chemical deicers – A review, *Water, Air, Soil Pollution*, **166**,49–63 (2005).
- [13] R. Kent and D. Andersen, Canadian water quality guidelines for glycols – An ecotoxicological review of glycols and associated aircraft anti-icing and deicing fluids, *Environ. Toxicol.* **14**, 481–522 (1999).
- [14] L. Boinovich and A. Emelyanenko, Anti-icing potential of superhydrophobic coatings, *Mendelev Commun.* **23**, 3–10(2013).

- [15] C. Antonini, M. Innocenti, T. Horn, M. Marengo, and A. Amirfazli, Understanding the effect of superhydrophobic coatings on energy reduction in anti-icing systems, *Cold Region Sci. Technol.* **67**, 58–67(2011).
- [16] L. Cao, A.K. Jones, V.K. Sikka, J. Wu, and D. Gao, Anti-icing superhydrophobic coatings., *Langmuir*. **25**, 12444–12448 (2009).
- [17] Z. Guo, W. Liu, and B.-L. Su, Superhydrophobic surfaces: From natural to biomimetic to functional, *J. Colloid Interface Sci.* **353**, 335–355 (2011).
- [18] P. Kim, T.-S. Wong, J. Alvarenga, M.J. Kreder, W.E. Adorno-Martinez, and J. Aizenberg, Liquid-infused nanostructured surfaces with extreme anti-ice and anti-frost performance., *ACS Nano*. **6**, 6569–6577 (2012).
- [19] Y. Cheng, D. Rodak, C. Wong, and C. Hayden, Effects of micro-and nano-structures on the self-cleaning behaviour of lotus leaves, *Nanotechnology*. **17**, 1359–1362 (2006).
- [20] Y. Liu, X. Chen, and J. Xin, Hydrophobic duck feathers and their simulation on textile substrates for water repellent treatment, *Bioinspir. Biomim.* **3**, 046007 (2008).
- [21] K. Koch, B. Bhushan, Y. Jung, and W. Barthlott, Fabrication of artificial Lotus leaves and significance of hierarchical structure for superhydrophobicity and low adhesion, *Soft Matter*. **5**, 1386–1393 (2009).
- [22] T.-S. Wong, T. Sun, L. Feng, and J. Aizenberg, Interfacial materials with special wettability, *MRS Bull.* **38**, 366–371 (2013)
- [23] T.-S. Wong, S.H. Kang, S.K.Y. Tang, E.J. Smythe, B.D. Hatton, A. Grinthal, and J. Aizenberg, Bioinspired self-repairing slippery surfaces with pressure-stable omniphobicity., *Nature*. **477**, 443–447 (2011).
- [24] N. Rungraeng, S.H. Yoon, Y. Li, and S. Jun, Development of a Self-Slippery Liquid-Infused Porous Surface (SLIPS) coating using carbon nanotube composite for repelling food debris and microbial biofilms, *Trans. ASABE*. **58**, 861–867 (2015).
- [25] A. Carré and K.L. Mittal (Eds.), *Superhydrophobic Surfaces*, CRC Press, Boca Raton, FL (2009).
- [26] P. Tourkine, M. Le Merrer, and D. Quéré, Delayed freezing on water repellent materials, *Langmuir*. **25**, 7214–7216 (2009).
- [27] L. Mishchenko, B. Hatton, and V. Bahadur, Design of ice-free nanostructured surfaces based on repulsion of impacting water droplets, *ACS Nano*. **4**, 7699–7707 (2010).
- [28] L. Makkonen, Ice adhesion—theory, measurements and countermeasures, *J. Adhesion Sci. Technol.* **26**, 413–445 (2012).
- [29] L. Makkonen, Surface melting of ice, *J. Phys. Chem. B*. **101**, 6196–6200 (1997).
- [30] A.J. Meuler, J.D. Smith, K.K. Varanasi, J.M. Mabry, G.H. McKinley, and R.E. Cohen, Relationships between water wettability and ice adhesion, *ACS Appl. Mater. Interfaces*. **2**, 3100–3110 (2010).
- [31] T. Young, An essay on the cohesion of fluids, *Philos. Trans. R. Soc. London*. **95**, 65–87(1805).
- [32] L.E. Raraty and D. Tabor, The adhesion and strength properties of ice, *Proc. R. Soc. London A* **245**, 184–201 (1958).
- [33] H. Saito, K. Takai, and G. Yamauchi, Water-and ice-repellent coatings, *Surf. Coatings Int. Part B*. **80**, 168–171 (1997).
- [34] Y.H. Yeong, A. Milionis, E. Loth, J. Sokhey, and A. Lambourne, Atmospheric ice adhesion on water-repellent coatings: wetting and surface topology effects, *Langmuir*. **31**, 13107–13116 (2015).

- [35] T. Bharathidasan, S.V. Kumar, M.S. Bobji, R.P.S. Chakradhar, and B.J. Basu, Effect of wettability and surface roughness on ice-adhesion strength of hydrophilic, hydrophobic and superhydrophobic surfaces, *Appl. Surf. Sci.* **314**, 241–250(2014).
- [36] H. Sojoudi, M. Wang, N.D. Boscher, G.H. McKinley, K.K. Gleason, Durable and scalable icephobic surfaces: similarities and distinctions from superhydrophobic surfaces, *Soft Matter*. **12**, 1938–1963(2016).
- [37] K.L. Mittal, The role of the interface in adhesion phenomena, *Polym. Eng. Sci.* **17**, 467–473 (1977).
- [38] C. Dorrer and J. Rühe, Some thoughts on superhydrophobic wetting, *Soft Matter*. **5**, 51–61 (2009).
- [39] A. Lafuma and D. Quéré, Superhydrophobic states., *Nat. Mater.* **2**, 457–460 (2003).
- [40] C. Antonini, F. Villa, and M. Marengo, Oblique impacts of water drops onto hydrophobic and superhydrophobic surfaces: outcomes, timing, and rebound maps, *Experiments in Fluids*. **55**, 1713 (9 pages) (2014).
- [41] S.A. Kulinich and M. Farzaneh, How wetting hysteresis influences ice adhesion strength on superhydrophobic surfaces, *Langmuir*. **25**, 8854–8856 (2009).
- [42] A. Meuler, G. McKinley, and R. Cohen, Exploiting topographical texture to impart icephobicity, *ACS Nano*. **4**, 7048–7052 (2010).
- [43] X. Yao, Y. Song, and L. Jiang, Applications of bio inspired special wettable surfaces, *Adv. Mater.* **23**, 719–734(2011).
- [44] T. Sun, L. Feng, X. Gao, and L. Jiang, Bioinspired surfaces with special wettability, *Acc. Chem. Res.* **38**, 644–652(2006).
- [45] A. Cassie and S. Baxter, Wettability of porous surfaces, *Trans. Faraday Soc.* **40**, 546–551(1944).
- [46] R. Wenzel, Resistance of solid surfaces to wetting by water, *Ind. Eng. Chem.* **28**, 988–994 (1936).
- [47] M. Nosonovsky and V. Hejazi, Why superhydrophobic surfaces are not always icephobic., *ACS Nano*. **6**, 8488–8491 (2012).
- [48] M.A. Sarshar, C. Swartz, S. Hunter, J. Simpson, and C.H. Choi, Effects of contact angle hysteresis on ice adhesion and growth on superhydrophobic surfaces under dynamic flow conditions, *Colloid Polym. Sci.* **291**, 427–435(2013).
- [49] K.K. Varanasi, T. Deng, J.D. Smith, M. Hsu, and N. Bhate, Frost formation and ice adhesion on superhydrophobic surfaces, *Appl. Phys. Lett.* **97**, 234102 (2010).
- [50] J. Lv, Y. Song, L. Jiang, and J. Wang, Bio-inspired strategies for anti-icing., *ACS Nano*. **8**, 3152–3169 (2014).
- [51] J. Soltis, J. Palacios, T. Eden, and D. Wolfe, Ice adhesion mechanisms of erosion-resistant coatings, *AIAA J.* **53**, 654–662(2015).
- [52] Y.H. Yeong, E. Loth, J. Sokhey, and A. Lambourne, Ice adhesion strength on hydrophobic and superhydrophobic coatings, AIAA-2014-2063, in: *Proc. 6th AIAA Atmospheric and Space Environment Conference* (2014).
- [53] H. Baker, W.D. Bascom, and C. Singleterry, The adhesion of ice to lubricated surfaces, *J. Colloid Sci.* **17**, 477–491(1962).
- [54] H.F. Bohn, and W. Federle, Insect aquaplaning: Nepenthes pitcher plants capture prey with the peristome, a fully wettable water-lubricated anisotropic surface, *Proc. Natl. Acad. Sci. (USA)* **101**, 14138–14143(2004).

- [55] A.K. Epstein, T.-S. Wong, R.A. Belisle, E.M. Boggs, and J. Aizenberg, Liquid-infused structured surfaces with exceptional anti-biofouling performance, *Proc. Natl. Acad. Sci. (USA)* **109**, 13182–13187(2012).
- [56] J. Chen, R. Dou, D. Cui, Q. Zhang, Y. Zhang, F. Xu, X. Zhou, J. Wang, Y. Song, and L. Jiang, Robust prototypical anti-icing coatings with a self-lubricating liquid water layer between ice and substrate, *ACS Appl. Mater. Interfaces*. **5**, 4026-4030 (2013).
- [57] S. Chernyy, M. Järn, K. Shimizu, A. Swerin, S.U. Pedersen, K. Daasbjerg, L. Makkonen, P. Claesson, and J. Iruthayaraj, Superhydrophilic polyelectrolyte brush layers with imparted anti-icing properties: effect of counter ions, *ACS Appl. Mater. Interfaces*. **6**, 6487–6496(2014).
- [58] P. Irajizad, M. Hasnain, N. Farokhnia, S.M. Sajadi, and H. Ghasemi, Magnetic slippery extreme icephobic surfaces, *Nat. Commun.* **7**, 13395(2016).
- [59] K. Golovin, S.P.R. Kobaku, D.H. Lee, E.T. DiLoreto, J.M. Mabry, and A. Tuteja, Designing durable icephobic surfaces, *Sci. Adv.* **2**, e1501496 (12 pages) (2016).
- [60] D.L. Beemer, W. Wang, A.K. Kota, M. Doi, F. Brochard-Wyart, A. Tuteja, J. Aizenberg, J. Wang, Y. Song, and L. Jiang, Durable gels with ultra-low adhesion to ice, *J. Mater. Chem. A*. **4**, 18253–18258 (2016).
- [61] R. Dou, J. Chen, Y. Zhang, X. Wang, D. Cui, Y. Song, L. Jiang, and J. Wang, Anti-icing coating with an aqueous lubricating layer, *ACS Appl. Mater. Interfaces*. **6**, 6998–7003(2014).
- [62] K. Varanasi, T. Deng, and J. Smith, Frost formation and ice adhesion on superhydrophobic surfaces, *Appl. Phys. Lett.* **97**, 8234102 (2010).
- [63] T. Maitra, M.K. Tiwari, C. Antonini, P. Schoch, S. Jung, P. Eberle, and D. Poulikakos, On the nanoengineering of superhydrophobic and impalement resistant surface textures below the freezing temperature, *Nano Lett.* **14**, 172–182 (2014).
- [64] Y. Liu, L. Li, H. Li, and H. Hu, An experimental study of surface wettability effects on dynamic ice accretion process over an UAS propeller model, *Aerospace Sci. Technol.* **73**, 164–172 (2018).
- [65] Q. Liu, Y. Yang, M. Huang, Y. Zhou, Y. Liu, and X. Liang, Durability of a lubricant-infused electro-spray silicon rubber surface as an anti-icing coating, *Appl. Surf. Sci.* **346**, 68–76 (2015).
- [66] N. Saleema, M. Farzaneh, R.W. Paynter, and D.K. Sarkar, Prevention of ice accretion on aluminum surfaces by enhancing their hydrophobic properties, *J. Adhesion Sci. Technol.* **25**, 27–40 (2011).
- [67] L. Gao, Y. Liu, L. Ma, and H. Hu, A hybrid strategy combining minimized leading-edge electric-heating and superhydro-/ice-phobic surface coating for wind turbine icing mitigation, *Renew. Energy*. **140**, 943–956(2019).
- [68] Y. Liu, C. Kolbaker, A.Y. Starikovskiy, R. Miles, and H. Hu, An experimental study on the thermal characteristics of NS-DBD plasma actuation and application for aircraft icing mitigation, *Plasma Sources Sci. Technol.* **28**, 014001(2019).
- [69] M. Nosonovsky, Materials science: slippery when wetted, *Nature*. **477**, 412–413 (2011).